Relationship Between MDCT-Imaged Myocardial Fat and Ventricular Tachycardia Substrate in Arrhythmogenic Right Ventricular Cardiomyopathy

Yuki Komatsu, MD;* Amir Jadidi, MD;* Frederic Sacher, MD, PhD; Arnaud Denis, MD; Matthew Daly, MD; Nicolas Derval, MD; Ashok Shah, MD; Heiko Lehrmann, MD; Chan-Il Park, MD; Reinhold Weber, MD; Thomas Arentz, MD; Gregor Pache, MD; Maxime Sermesant, PhD; Nicholas Ayache, PhD; Jatin Relan, PhD; Michel Montaudon, MD, PhD; François Laurent, MD; Mélèze Hocini, MD; Michel Haïssaguerre, MD; Pierre Jaïs, MD; Hubert Cochet, MD, PhD

Background—Myocardial fibrofatty infiltration is a milieu for ventricular tachycardia (VT) in arrhythmogenic right ventricular cardiomyopathy (ARVC) and can be depicted as myocardial hypodensity on contrast-enhanced multidetector computed tomography (MDCT) with high spatial and temporal resolution. This study aimed to assess the relationship between MDCT-imaged myocardial fat and VT substrate in ARVC.

Methods and Results—We studied 16 patients with ARVC who underwent ablation and preprocedural MDCT. High-resolution imaging data were processed and registered to high-density endocardial and epicardial maps in sinus rhythm on 3-dimensional electroanatomic mapping (3D-EAM) (626±335 and 575±279 points/map, respectively). Analysis of the locations of low-voltage and fat segmentation included the following endocardial and epicardial regions: apex, mid (anterior, lateral, inferior), and basal (anterior, lateral, inferior). The location of local abnormal ventricular activities (LAVA) was compared with fat distribution. RV myocardial fat was successfully segmented and integrated with 3D-EAM in all patients. The κ agreement test demonstrated a good concordance between the epicardial low voltage and fat (κ=0.69, 95% CI 0.54 to 0.84), but fair concordance with the endocardium (κ=0.41, 95% CI 0.27 to 0.56). The majority of LAVA (520/653 [80%]) were located within the RV fat segmentation, of which 90% were not farther than 20 mm from its border. Registration of MDCT allowed direct visualization of the coronary arteries, thus avoiding coronary damage during epicardial radiofrequency delivery.

Conclusions—The integration of MDCT-imaged myocardial fat with 3D-EAM provides valuable information on the extent and localization of VT substrate and demonstrates ablation targets clustering in its border region. (***J Am Heart Assoc***. 2014;3: e000935 doi: 10.1161/JAHA.114.000935)

Key Words: ablation • arrhythmia • arrhythmogenic right ventricular cardiomyopathy • electroanatomic mapping • imaging • ventricular tachycardia

Arrhythmogenic right ventricular cardiomyopathy (ARVC) is an inherited desmosomal cardiomyopathy characterized by fibrofatty replacement of the right ventricular (RV) myocardium.[1,2] Fibrofatty infiltration provides an ideal milieu for life-threatening ventricular tachycardia (VT). Although myocyte loss of the RV with fibrofatty replacement is a pathological hallmark of ARVC, its relationship with arrhythmia substrate as assessed by 3-dimensional electroanatomic mapping (3D-EAM) has not been fully investigated. Contrast-enhanced multidetector computed tomography (MDCT) can identify intramyocardial fat depicted as myocardial hypodensity with high spatial resolution.[3,4] The purpose of this study was to introduce the method of integration of MDCT-imaged myocardial fat with 3D-EAM and to assess the

relationship between the RV myocardial fat and VT substrate in ARVC.

Methods

Study Population

Sixteen patients with ARVC (13 men, 41±17 years old) who underwent both catheter ablation of VT and preprocedural MDCT at 2 institutions were enrolled in this study. All patients were diagnosed as definite ARVC according to the 2010 Revised Task Force Criteria.[1] All patients had evidence of sustained VTs with left-bundle-branch-block morphology. Patients with repetitive premature ventricular contractions or nonsustained VT in the absence of sustained VT were excluded. Three patients had undergone a prior ablation procedure. This study was approved by institutional review committees of each institution, and all patients gave their informed consent.

MDCT Image Acquisition and Processing

Cardiac MDCT was performed using a contrast-enhanced cardiac-gated method on a 64-slice scanner (Somatom Definition; Siemens, Forchheim, Germany). Images were acquired during the first pass of 120 mL iodine contrast media injected using a biphasic protocol adapted to the study of RV wall (ie, 60 mL of iodine contrast at the rate of 5 mL/s followed by 120 mL of a 50:50 mixture of saline and contrast media, also at the rate of 5 mL/s). Typical parameters were the following: gantry rotation time 330 ms, temporal resolution 83 ms, collimation 64×0.6 mm, tube voltage 100 to 120 kV, typical tube current 600 mAs with a dose modulation protocol. Images were reconstructed at end-diastole in a series of contiguous 1-mm-thick short-axis slices encompassing the whole RV from base to apex. Typical in-plane resolution was 0.4×0.4 mm. Image segmentation and fat quantification were performed using an in-house method developed as a plugin of the software OsiriX3.6.1 (OsiriX Foundation, Geneva, Switzerland). The image processing strategy is illustrated in Figure 1. After manual definition of tricuspid and pulmonary planes, the RV endocardium was automatically segmented using region growing. The lower-density threshold applied for region growing was set 3 SD above mean myocardial density, as assessed by drawing a 3-cm^2 region of interest in the interventricular septum at mid-ventricular level. A 2-mm-thick RV free wall layer was then automatically derived from RV endocardial segmentation using a dilatation operator. Myocardial hypodensity was automatically segmented in the RV free wall by using histogram thresholding, the cut-off for fat being defined as pixel density<-10 HU. The extent of fat was expressed in percent of RV free wall. Segmented images were used to generate 3-dimensional meshes compatible with 3D-EAM systems using the software MUSIC (Multimodality software for specific imaging in cardiology, Liryc Institute, University of Bordeaux, Inria Sophia-Antipolis, France). In addition to RV and fat, patient-specific models also integrated manual segmentations of coronary sinus in order to facilitate registration, and coronary arteries in order to guide potential epicardial ablation.

Electroanatomical Mapping

All anti-arrhythmic drugs except amiodarone were discontinued for at least 5 half-lives before the ablation. Epicardial access was secured through a subxiphoid puncture. The decision to proceed to epicardial mapping and ablation was left to the operator's discretion. EAM was performed during sinus rhythm using CartoV3 (Biosense-Webster, Diamond Bar, CA) in 12 patients or NavX (Ensite NavX, St Jude Medical, St. Paul, MN) in 4 patients. Mapping was performed with a multipolar high-density mapping catheter (PentaRayNav; Biosense Webster). We defined a peak-to-peak bipolar amplitude of <1.5 mV as the bipolar low-voltage zone and unipolar amplitude <5.5 mV as the low unipolar voltage.[5–8]

Image Integration With 3D-EAM

After the acquisition of endocardial and epicardial geometries, 3D-EAM geometry was registered with the imported MDCT model. Identifiable anatomic reference points (coronary sinus, RV apex, and tricuspid annulus [3, 6, 9, and 12 o'clock]) were used as landmarks for alignment and orientation of the 3D-EAM and imaging models. A decapolar catheter (2-5-2 mm, Xtrem; ELA Medical, Montrouge, France) was placed in the coronary sinus, with distal electrodes in the great cardiac vein. The body of the coronary sinus catheter was taped to provide a stable spatial reference, and a discreet anatomic boundary for guidance of the 3D-EAM/imaging model registration that could be monitored fluoroscopically throughout the procedure. When using Carto, after initial alignment using these fixed reference points as landmarks for registration, automatic surface registration using CartoMerge (Biosense Webster) was performed. The NavX Fusion registration algorithm allowed dynamic molding of the 3D-EAM geometry to the static MDCT surface. After primary registration, the registered model was refined using a second set of fiducial points, judiciously placed in a stepwise fashion to further align both surfaces at sites of local mismatch.[9]

Radiofrequency Ablation

Programmed ventricular stimulation from the RV apex was performed at a basic drive cycle length of 600 and 400 ms
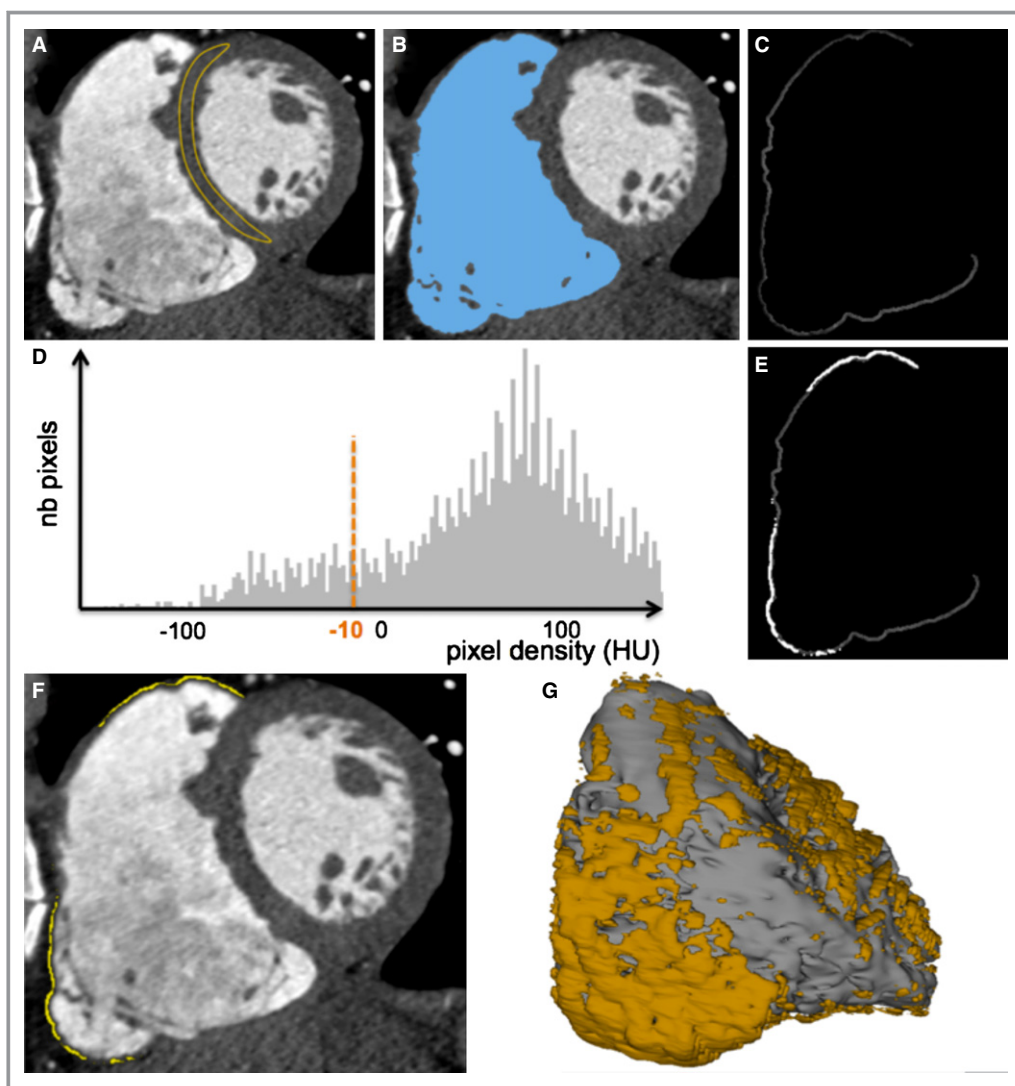
Figure 1. Method for the segmentation of myocardial fat from MDCT images. On contrast-enhanced ECG-gated cardiac images reformatted in short axis, a region of interest is drawn on the interventricular septum to assess normal myocardial density (A). The RV endocardium is automatically segmented using region-growing segmentation with a lower density cut-off 3 SD above mean myocardial density (B). A 2-mm-thick RV free wall is derived from this segmentation using a dilatation operator (C). Myocardial fat is segmented on the histogram as pixels with density <-10 HU (D through F). Segmented images are then used to compute 3D objects compatible with 3D-EAM systems (G). 3D-EAM indicates 3-dimensional electroanatomic mapping; MDCT, multidetector computed tomography; RV, right ventricle.

with up to triple extrastimuli decrementally down to 200 ms or up to ventricular refractoriness, whichever occurred first. When VT was inducible and hemodynamically tolerated, ablation was guided by conventional activation and entrainment mapping. The critical sites of VT were defined as the sites where presystolic or mid-diastolic electrograms were present and possibly showed good entrainment, long S-QRS and/or VT termination during radiofrequency delivery, followed by noninducibility of the VT that was reproducibly inducible before. After restoration of sinus rhythm, further ablation targeting local abnormal ventricular activities (LAVA) was performed in all patients. LAVA were defined as

previously described.[10,11] In patients with noninducible or poorly tolerated VT, ablation of LAVA was performed during sinus rhythm. The location of LAVA and critical site of VT reentry circuit were documented and tagged on the 3D-EAM.

Radiofrequency energy was delivered with a 3.5-mm open-irrigation catheter (Thermocool; Biosense Webster) with a power of 30 to 45 W endocardially, and 25 to 35 W epicardially. If both endocardial and epicardial LAVA were detected, ablation was always performed initially on the endocardial side in an attempt to abolish the potentials transmurally, followed by subsequent epicardial ablation if needed.[12] Induction of VT was repeated with programmed

stimulation using the same protocol as pre-ablation induction. The ideal procedural endpoint was complete elimination of LAVA and noninducibility.

Statistical Analysis

Categorical variables were expressed as numbers and percentages, and were compared using χ^2 test or Fisher's exact test, as appropriate. Continuous data were expressed as mean±SD for normally distributed variables and were compared using unpaired t test. As the electrogram characteristics were non-normally distributed variables, they were expressed as median [25th to 75th percentiles] and were compared using Mann–Whitney U-test. For assessing the correlation between the extent of fat in RV free wall and the size of low-voltage region, Pearson correlation coefficients were calculated. The analysis of the locations of low voltage on the electroanatomic maps and MDCT-derived RV fat included the following 7 regions in both endo- and epicardium: apex, mid (anterior, lateral, inferior), and basal (anterior, lateral, inferior). The concordance between the low voltage and RV fat in each region was assessed by the Cohen κ agreement test. All tests were 2-tailed, and $P<0.05$ was considered statistically significant.

Results

Clinical Characteristics

Patient characteristics are summarized in Table 1. All patients met the revised diagnostic criteria for definite ARVC.[1] Three patients had a family history of ARVC or premature (aged <40 years) sudden death due to proven or suspected ARVC. Patients had the following symptoms: syncope (38%), presyncope (19%), and palpitations (31%). On echocardiography, all patients had global or regional RV dysfunction. All patients had episodes of repetitive, sustained VT, resistant to antiarrhythmic drug therapy, requiring either external cardioversion or implantable cardioverter defibrillator therapy. Holter monitor detected nonsustained VT in 4 (25%) patients and frequent premature ventricular contraction (>1000/24 hours) in 12 (75%) including monomorphic premature ventricular contractions in 5 (31%) and polymorphic premature ventricular contractions in 7 (44%). Mean RV end-diastolic volume, which was derived from endocardial segmentation and expressed in mL/m^2 body surface area, was 129±30 mL/m^2.

Electroanatomic Mapping

Mapping data are summarized in Table 2. Detailed RV mapping was performed endocardially in all 16 and

Table 1. Characteristics of Study Population

	N=16
Age, y	41±17
Male/female	13/3
LV ejection fraction, %	60±7
ICD	14 (88%)
Medications	
Amiodarone	11 (69%)
β-Blocker	14 (88%)
Family history	3 (19%)
Endomyocardial biopsy performed	0 (0%)
Clinical symptom	
Syncope	6 (38%)
Presyncope	3 (19%)
Palpitations	5 (31%)
ECG abnormalities	
Epsilon wave	4 (25%)
Inverted T waves V1 to 2	2 (13%)
Inverted T waves V1 to 3 or beyond	8 (50%)
QRS duration ≥110 ms (V1 to 2)	7 (44%)
TAD ≥55 ms	4 (25%)
Ventricular arrhythmia at Holter monitor	
Frequent PVCs (>1000/24 h)	12 (75%)
Monomorphic PVCs	5 (31%)
Polymorphic PVCs	7 (44%)
Nonsustained VT	4 (25%)
Structural evaluation	
RV dilatation/dysfunction	16 (100%)
RVEDV/BSA, mL/m^2	129±30
LV involvement	2 (13%)

BSA indicates body surface area; ICD, implantable cardioverter defibrillator; LV, left ventricle; PVC, premature ventricular contraction; RV, right ventricle; RVEDV, right ventricular end-diastolic volume; TAD, terminal activation duration; VT, ventricular tachycardia.

epicardially in 13 patients. The average number of mapping points was 626±335 and 575±279 points/map in the RV endocardium and epicardium, respectively. The bipolar low-voltage area was significantly smaller in the endocardium than the epicardium (46.6±28.6 cm^2 versus 115.3±32.2 cm^2, $P<0.05$). The most common location of epicardial low voltage was basal lateral (12 [92%] patients), followed by the basal anterior (9 [69%] patients) and basal inferior region (9 [69%] patients). Endocardial low-voltage regions were mainly found at the basal inferior (12 [75%] patients) and basal lateral regions (12 [75%] patients). The vast majority of endocardial low-voltage regions (96%) were located within an opposite

Table 2. MDCT and Mapping Data

Pt	MDCT		Mapping	Mapping Points		Low Voltage Area (cm²)		LAVA Location
	RVEDV/BSA (mL/m²)	RV Free Wall Fat (%)	Mapping	Endo	Epi	Endo	Epi	LAVA Location
1	150.33	11.35	Endo	1038	NA	23	NA	Endo (basal Inf)
2	153.78	18.21	Endo+Epi	1040	414	31.4	154.3	Endo (basal Inf), Epi (basal Ant, Inf)
3	91.82	17.43	Endo+Epi	461	1351	57.7	139	Endo (basal Inf), Epi (basal Ant, Inf)
4	126.97	11.63	Endo+Epi	725	584	36.7	150.5	Endo (basal Inf, Lat), Epi (basal Lat)
5	144.93	21.01	Endo+Epi	375	821	64.7	120.6	Endo (basal/mid Lat), Epi (basal/mid Lat)
6	74.29	19.79	Endo+Epi	220	580	21.1	97.6	Epi (basal Lat)
7	172.25	18.64	Endo+Epi	845	501	84.3	130.5	Endo (basal Ant), Epi (basal Ant)
8	160.82	12.72	Endo+Epi	301	331	60.2	104	Endo (basal Inf, Lat), Epi (basal Ant, Lat)
9	146.52	22.51	Endo+Epi	327	234	70.7	168.2	Endo (basal Ant, Lat), Epi (basal Ant, Lat)
10	84.23	9.69	Endo+Epi	1201	462	40.7	121	Endo (basal Inf), Epi (basal Inf)
11	135.92	12.85	Endo+Epi	510	667	2.3	63.7	Epi (basal Ant)
12	97.53	10.88	Endo+Epi	278	654	2	84.1	Epi (apex, basal Ant, Lat)
13	152.32	13.50	Endo+Epi	435	415	73.6	100.6	Endo (basal Inf, Lat), Epi (basal Inf, Lat)
14	152.95	18.73	Endo	650	NA	70.5	NA	Endo (apex, mid Ant, basal Inf)
15	111.76	21.53	Endo	1172	NA	90	NA	Endo (apex, basal Lat)
16	114.64	8.58	Endo+Epi	445	467	16	65	Endo (basal Inf), Epi (basal Inf)

BSA indicates body surface area; Endo, endocardium; Epi, epicardium; LAVA, local abnormal ventricular activities; MDCT, multidetector computed tomography; RVEDV, right ventricular endo-diastolic volume.

epicardial low-voltage region, suggesting fibrofatty replacement starting from the epicardium and spreading endocardially. LAVA were found in all patients. The number of electrograms exhibiting LAVA was 17.3 ± 19.6 per map on the endocardium, and 29.0 ± 21.2 on the epicardium. These LAVA occupied 8.4 ± 5.5 cm² and 14.2 ± 6.5 cm² on the endocardial and epicardial surfaces, respectively.
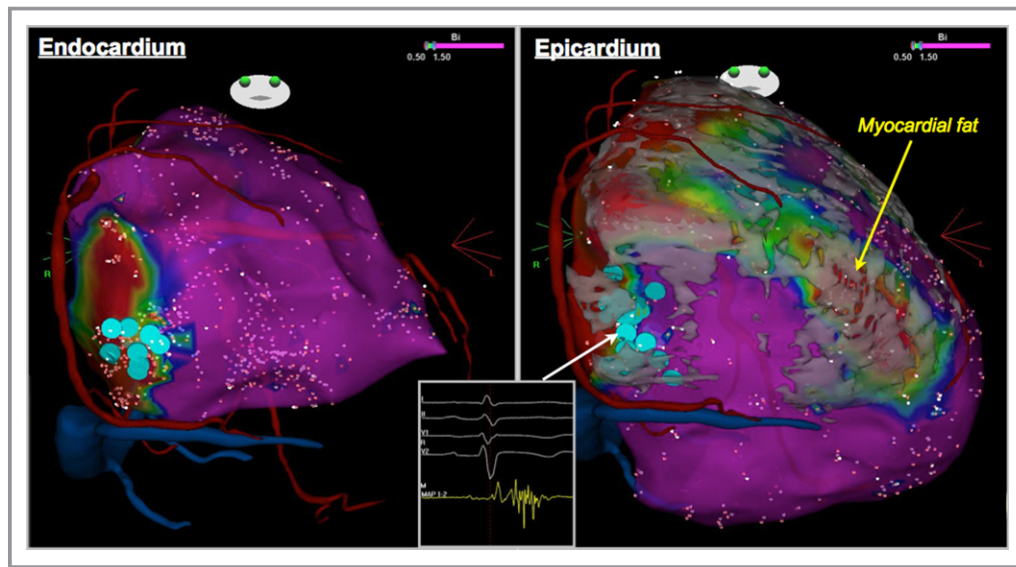
RV Myocardial Fat at MDCT

RV fat imaged by contrast-enhanced MDCT could be identified and successfully integrated with 3D-EAM in all patients. The RV fat segmentation was identified in the following regions: apex in 10/16 (63%), midanterior in 11/16 (69%), midlateral in 3/16 (19%), midinferior in 3/16 (19%), basal-anterior in 12/16 (75%), basal-lateral in 15/16 (94%), and basal-inferior in 15/16 (94%). The extent of fat in RV free wall fat was $15.6\pm4.6\%$.

Relation Between RV Fat and Low-Voltage Area

There was a positive correlation between the extent of fat in RV free wall and the size of the low-voltage region on both endocardium ($r=0.61$, $P=0.012$) and epicardium ($r=0.57$,

$P=0.042$). Figure 2 shows endo- and epicardial voltage maps demonstrating the spatial correlation between RV fat and low-voltage zones. The topographical comparison between RV fat and bipolar low-voltage areas on the epicardium showed a high concordance, which was assessed by the κ agreement test ($\kappa=0.69$, 95% CI 0.54 to 0.84). On the endocardium, however, the κ agreement test demonstrated a lower concordance between a bipolar low voltage and RV fat ($\kappa=0.41$, 95% CI 0.27 to 0.56). There was mismatch in 32 fat regions (32/69 [46.4%]) where endocardial EAM did not demonstrate a bipolar low voltage. In contrast, there was a high concordance between the endocardial unipolar low-voltage region and RV fat ($\kappa=0.65$, 95% CI 0.49 to 0.81).

The sensitivity, specificity, positive predictive value, and negative predictive value of MDCT-imaged RV fat to identify bipolar low voltage were 92.5%, 55.6%, 53.6%, and 93.0% on the endocardium, respectively, and 93.6%, 75.0%, 80%, and 91.7% on the epicardium, respectively (Table 3). Presence of both endocardial unipolar low-voltage and MDCT-derived RV fat was able to predict epicardial low-voltage scar with the sensitivity of 89.4%, specificity of 86.4%, positive predictive value of 87.5%, and negative predictive value of 88.4%.

Figure 2. Endocardial and epicardial voltage maps with merged MDCT model. The segmentation of RV myocardial fat superimposed on the electroanatomic map on the epicardium showed a good match with the low-voltage area. LAVA were distributed at the basal-inferior area on both endo- and epicardium (blue dots), which corresponded to the border of fat segmentation. LAVA indicates local abnormal ventricular activities; MDCT, multidetector computed tomography; RV, right ventricle.

RV Fat and LAVA

A total of 653 LAVA (276 endocardial and 377 epicardial) were identified and reviewed from all study subjects. The majority of LAVA (520/653 [80%]) were located within the RV fat segmentation. Of these, 466 LAVA were detected within 20 mm of the border of RV fat. Although 133 (20%) LAVA were located outside the RV fat segmentation, 125 of them were no farther than 20 mm from its border. Therefore, the border area of the RV fat segmentation harbored the vast majority of LAVA (591/653 [91%]) (Figures 2 and 3). LAVA within the RV fat demonstrated significantly lower amplitude than those outside (endocardium: 0.32 mV [0.21, 0.51 mV] versus 0.50 mV [0.35, 0.81 mV], $P<0.001$; epicardium: 0.49 mV [0.22, 0.96 mV] versus 0.75 mV [0.37, 1.55 mV], $P<0.001$). The electrogram duration of abnormal signals, as estimated by the interval from the onset of far-field potential to the end of LAVA, was significantly longer inside the RV fat than outside (endocardium: 117 ms [101, 149 ms] versus 109 ms [91, 131 ms], $P=0.021$; epicardium: 112 ms [91, 153 ms] versus 94 ms [83, 117 ms], $P<0.001$).

Ablation Results

In total, 8 sustained VTs (induced or spontaneous) were hemodynamically stable and mapped. All critical sites were confirmed at the epicardium and labeled on the 3D-EAM. All but 1 of the critical sites were located within the RV fat: at the border of RV fat segmentation (within 20 mm from the edge) in 6 sites, and deep inside fat segmentation in 1 site. Registration of MDCT data allowed direct visualization of coronary arteries and helped avoid coronary damage during epicardial radiofrequency delivery. Of 13 patients undergoing epicardial mapping, 6 (46%) had epicardial basal inferolateral LAVA located close to the right coronary arteries (within 5 mm) (Figure 3). Endocardial ablation abolished epicardial LAVA completely in 2 cases, and partially in 9 cases. Two patients had LV involvement and low-voltage scar in the LV epicardium. However, radiofrequency was not delivered because there was no LAVA in the LV scar. Mean radiofrequency delivery time and procedure time was 36±15 and 287±26 minutes, respectively. There were no complications. Combined endpoint of noninducibility of any VT and complete LAVA elimination was achieved in 11

Table 3. Agreement Analysis of MDCT-Derived Fat Segmentation for Detection of Low-Voltage Regions

	Sensitivity	Specificity	Positive Predictive Value	Negative Predictive Value
Endocardium (n=112)	92.5%	55.6%	53.6%	93.0%
Epicardium (n=91)	93.6%	75.0%	80.0%	91.7%

MDCT indicates multidetector computed tomography.
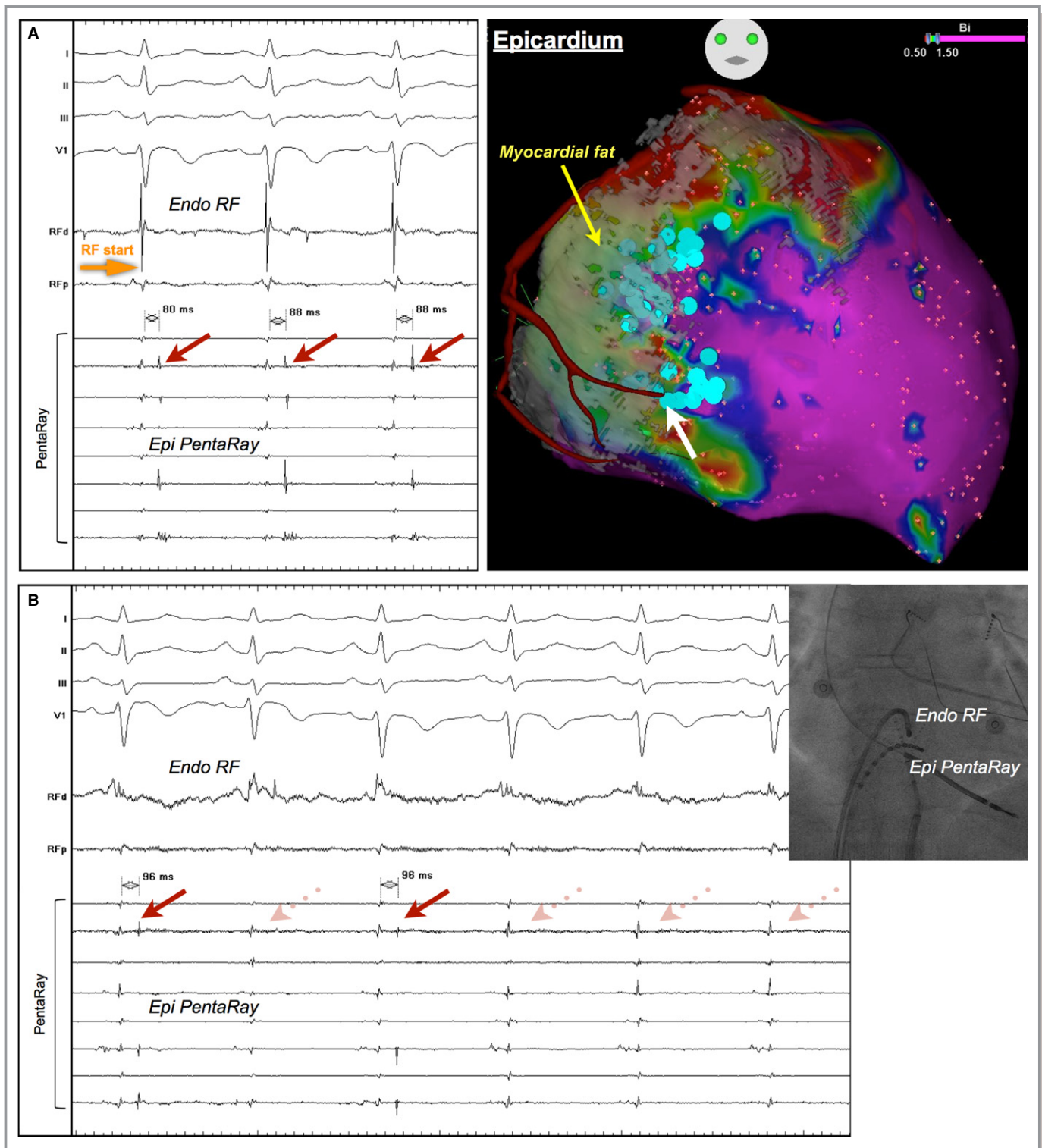
Figure 3. Epicardial LAVA near the coronary artery eliminated by endocardial ablation. The location of epicardial low voltage correlated to the RV myocardial fat. LAVA were identified near the border of fat segmentation (blue dots). There were LAVA near the branch of the right coronary artery (white arrow). Radiofrequency (RF) energy was delivered at the facing endocardial site (A). Epicardial LAVA were eliminated transmurally during endocardial ablation (B). LAVA indicates local abnormal ventricular activities; RV, right ventricle.

patients. During median follow-up of 9 months [5, 19 months], 12 (75%) patients were free from VT recurrence. VT recurrence was observed in 1 of 11 patients (9%) who achieved combined end point. In contrast, VT recurrence was observed in 3 of 5 patients (60%) who failed to reach the end point.

Discussion

Main Findings

This study is the first to demonstrate the feasibility of integrating MDCT-derived RV fat into a 3-D navigation system and to evaluate its relationship with VT substrate in ARVC. There are 3 key findings: (1) a positive correlation between the extent of fat in RV free wall as imaged by MDCT and low-voltage area; (2) a high concordance between the location of RV fat and low voltage in the epicardium, but fair concordance in the endocardium with fewer low-voltage regions compared to the RV fat at MDCT; and (3) the vast majority of LAVA located around the border of the RV fat segmentation.

Cardiac Imaging Methods in ARVC

Cardiac magnetic resonance is currently the main imaging tool in the diagnostic workup of ARVC. Current diagnostic criteria have focused on the measurement of RV end-diastolic volume and RV ejection fraction with the use of magnetic resonance imaging.[1] Myocyte loss of the RV with fibrofatty replacement is a pathological hallmark of ARVC and can be depicted as low density as compared to the myocardium on contrast-enhanced cardiac MDCT. However, this imaging feature is not part of current recommendations for the diagnosis of ARVC because of the poor reproducibility of visual analysis, and because intramyocardial fat in RV free wall is not specific of ARVC.[13,14]

Previous imaging studies have demonstrated the lack of delayed enhancement at magnetic resonance imaging in a significant proportion (ranging from 33% to 61%) of ARVC patients fulfilling task-force diagnostic criteria.[14–17] One prior study demonstrated that delayed gadolinium enhancement at magnetic resonance imaging may be less sensitive than electrophysiological scar as assessed by 3D-EAM to detect VT substrate.[15] Once patients fulfilling task-force diagnostic criteria are referred for ablation of recurrent VT, an image integration approach with high sensitivity and low false-negative recognition of arrhythmia substrate is endorsed as a useful supplemental technique to guide mapping and ablation of VT in ARVC patients. Of note, the present technique of MDCT image integration was able to visualize the extent and distribution of arrhythmia substrate in the entire study cohort. In this study, we chose to use MDCT rather than magnetic resonance imaging because high blood-pool densities allow for automatic endocardial segmentation,[18] and because high spatial resolution is required to study the thin RV wall. The choice of a 2-mm wall thickness in which myocardial densities were analyzed was based on a previous report describing the normal value of RV wall thickness.[19] Any fat found <2 mm from the endocardium can be considered as abnormal, related to either intramyocardial fat or severe wall thinning.

RV Fat and Electrophysiological Scar

The presence of RV fat demonstrated a higher degree of spatial correlation with low voltage on the epicardium than on the endocardium. This is in line with the fact that VT substrate in ARVC predominantly distributes on the epicardium because the fibrofat replacement starts from the epicardium and proceeds to endocardium.[20,21] Despite this, there was a positive correlation between the extent of the RV free wall fat as estimated by MDCT and the size of low voltage on the endocardium as well as on the epicardium. These findings suggest that the MDCT-derived fat information allows the preprocedural expectation of the electrophysiological scar extent on both endocardium and epicardium.

RV Fat and LAVA Distribution

This study found a good correlation of LAVA location with RV fat segmentation superimposed on the 3D-EAM. Interestingly, the majority of LAVA were found not deep inside fat segmentation but at its border. This runs contrary to postinfarction VT, where most of the delayed components of abnormal signals disperse in the dense scar.[22] This observation might be related to a difference between RV and LV rather to an intrinsic difference between ischemic and dysplastic substrates. Indeed, since RV thickness is far thinner than LV thickness, there is less room within the wall for slow-conducting channels to penetrate deep inside the substrate as it has been described in postinfarction VT.[9,22] Our findings suggest that dense fibrofatty replacement may lack the surviving myocyte bundles responsible for generation and perpetuation of VT. The border of the fat segmentation may be more likely to harbor heterogeneous fibrofatty infiltration with islets of surviving myocytes surrounded by the fibrous tissue, which provides an ideal substrate for VT. Our findings may be supported by a prior study wherein the predictors of the incidence of VT were not the extent of RV scar size but the presence of fragmented and delayed electrograms at 3D-EAM.[23]

Another possible reason for a clustering of LAVA on substrate edges may be due to methodological limitation. The method proposed in the current study would intrinsically miss any substrate located > 2 mm from the endocardium. Therefore, LAVA observed in a healthy area surrounding MDCT-defined substrate are likely to be related to subepicardial substrate of limited transmurality in an area where RV wall thickness is >2 mm.

Clinical Implications

This study demonstrates that arrhythmia substrate can be assessed noninvasively with the use of MDCT, allowing for a preprocedural recognition of the specific distribution of

LAVA as well as electrophysiologic scar. This image-integration technique can therefore help focus mapping on the culprit region. In addition, the integration of MDCT data with 3D-EAM also provides information regarding the location of coronary arteries. A previous study has described that direct visualization of the location of the coronary vessels, provided by contrast-enhanced MDCT angiographic data with high resolution, may increase safety by warning the operator when to withhold epicardial radiofrequency.[24,25] LAVA in ARVC are often located in the epicardial basal inferolateral region where radiofrequency delivery has the risk of right coronary artery damage. In our series, this issue occurred in 6 of 13 (46%) of the patients. In these cases, endocardial ablation to transmurally abolish LAVA from the opposite epicardial site can be useful to minimize the risk.[12]

Study Limitations

This study was undertaken on the 2 most widely used 3D-EAM systems, which differ in terms of registration methods. However, we confirmed that the present technique was feasible in both systems and that our findings were consistent among patients. Furthermore, a previous report described a strong correlation between low-voltage area determined by Carto and NavX.[26]

Conclusions

Integration of MDCT-imaged myocardial fat into 3D-EAM is feasible in patients with ARVC. Its segmentation superimposed on 3D-EAM provides valuable information to recognize the extent and specific distribution of VT substrate and demonstrates ablation targets clustering in its border zone.

Sources of Funding

Disclosures

None.

References

1. Marcus FI, McKenna WJ, Sherrill D, Basso C, Bauce B, Bluemke DA, Calkins H, Corrado D, Cox MG, Daubert JP, Fontaine G, Gear K, Hauer R, Nava A, Picard MH, Protonotarios N, Saffitz JE, Sanborn DM, Steinberg JS, Tandri H, Thiene G, Towbin JA, Tsatsopoulou A, Wichter T, Zareba W. Diagnosis of arrhythmogenic right ventricular cardiomyopathy/dysplasia: proposed modification of the task force criteria. *Circulation*. 2010;121:1533–1541.

2. Jacoby D, McKenna WJ. Genetics of inherited cardiomyopathy. *Eur Heart J*. 2012;33:296–304.

3. Soh EK, Villines TC, Feuerstein IM. Sixty-four-multislice computed tomography in a patient with arrhythmogenic right ventricular dysplasia. *J Cardiovasc Comput Tomogr*. 2008;2:191–192.

4. Tandri H, Bomma C, Calkins H, Bluemke DA. Magnetic resonance and computed tomography imaging of arrhythmogenic right ventricular dysplasia. *J Magn Reson Imaging*. 2004;19:848–858.

5. Corrado D, Basso C, Leoni L, Tokajuk B, Bauce B, Frigo G, Tarantini G, Napodano M, Turrini P, Ramondo A, Daliento L, Nava A, Buja G, Iliceto S, Thiene G. Three-dimensional electroanatomic voltage mapping increases accuracy of diagnosing arrhythmogenic right ventricular cardiomyopathy/dysplasia. *Circulation*. 2005;111:3042–3050.

6. Marchlinski FE, Zado E, Dixit S, Gerstenfeld E, Callans DJ, Hsia H, Lin D, Nayak H, Russo A, Pulliam W. Electroanatomic substrate and outcome of catheter ablative therapy for ventricular tachycardia in setting of right ventricular cardiomyopathy. *Circulation*. 2004;110:2293–2298.

7. Verma A, Kilicaslan F, Schweikert RA, Tomassoni G, Rossillo A, Marrouche NF, Ozduran V, Wazni OM, Elayi SC, Saenz LC, Minor S, Cummings JE, Burkhardt JD, Hao S, Beheiry S, Tchou PJ, Natale A. Short- and long-term success of substrate-based mapping and ablation of ventricular tachycardia in arrhythmogenic right ventricular dysplasia. *Circulation*. 2005;111:3209–3216.

8. Polin GM, Haqqani H, Tzou W, Hutchinson MD, Garcia FC, Callans DJ, Zado ES, Marchlinski FE. Endocardial unipolar voltage mapping to identify epicardial substrate in arrhythmogenic right ventricular cardiomyopathy/dysplasia. *Heart Rhythm*. 2011;8:76–83.

9. Komatsu Y, Cochet H, Jadidi A, Sacher F, Shah A, Derval N, Scherr D, Pascale P, Roten L, Denis A, Ramoul K, Miyazaki S, Daly M, Riffaud M, Sermesant M, Relan J, Ayache N, Kim S, Montaudon M, Laurent F, Hocini M, Haïssaguerre M, Jaïs P. Regional myocardial wall thinning at multidetector computed tomography correlates to arrhythmogenic substrate in postinfarction ventricular tachycardia: assessment of structural and electrical substrate. *Circ Arrhythm Electrophysiol*. 2013;6:342–350.

10. Jaïs P, Maury P, Khairy P, Sacher F, Nault I, Komatsu Y, Hocini M, Forclaz A, Jadidi AS, Weerasooriya R, Shah A, Derval N, Cochet H, Knecht S, Miyazaki S, Linton N, Rivard L, Wright M, Wilton SB, Scherr D, Pascale P, Roten L, Pederson M, Bordachar P, Laurent F, Kim SJ, Ritter P, Clementy J, Haïssaguerre M. Elimination of local abnormal ventricular activities: a new end point for substrate modification in patients with scar-related ventricular tachycardia. *Circulation*. 2012;125:2184–2196.

11. Komatsu Y, Daly M, Sacher F, Derval N, Pascale P, Roten L, Scherr D, Jadidi A, Ramoul K, Denis A, Jesel L, Zellerhoff S, Lim HS, Shah A, Cochet H, Hocini M, Haïssaguerre M, Jaïs P. Electrophysiologic characterization of local abnormal ventricular activities in post-infarction ventricular tachycardia with respect to their anatomical location. *Heart Rhythm*. 2013;10:1630–1637.

12. Komatsu Y, Daly M, Sacher F, Cochet H, Denis A, Derval N, Jesel L, Zellerhoff S, Lim HS, Jadidi A, Nault I, Shah A, Roten L, Pascale P, Scherr D, Aurillac-Lavignolle V, Hocini M, Haissaguerre M, Jais P. Endocardial ablation to eliminate epicardial arrhythmia substrate in scar-related ventricular tachycardia. *J Am Coll Cardiol*. 2014;63:1416–1426.

13. Bomma C, Rutberg J, Tandri H, Nasir K, Roguin A, Tichnell C, Rodriguez R, Kasper E, Spevak P, Bluemke DA, Calkins H. Misdiagnosis of arrhythmogenic right ventricular dysplasia/cardiomyopathy. *J Cardiovasc Electrophysiol*. 2004;15:300–306.

14. Sen-Chowdhry S, Prasad SK, Syrris P, Wage R, Ward D, Merrifield R, Smith GC, Firmin DN, Pennell DJ, McKenna WJ. Cardiovascular magnetic resonance in arrhythmogenic right ventricular cardiomyopathy revisited: comparison with task force criteria and genotype. *J Am Coll Cardiol*. 2006;48:2132–2140.

15. Marra MP, Leoni L, Bauce B, Corbetti F, Zorzi A, Migliore F, Silvano M, Rigato I, Tona F, Tarantini G, Cacciavillani L, Basso C, Buja G, Thiene G, Iliceto S, Corrado D. Imaging study of ventricular scar in arrhythmogenic right ventricular cardiomyopathy: comparison of 3D standard electroanatomical voltage mapping and contrast-enhanced cardiac magnetic resonance. *Circ Arrhythm Electrophysiol*. 2012;5:91–100.

16. Tandri H, Saranathan M, Rodriguez ER, Martinez C, Bomma C, Nasir K, Rosen B, Lima JA, Calkins H, Bluemke DA. Noninvasive detection of myocardial fibrosis in arrhythmogenic right ventricular cardiomyopathy using delayed-enhancement magnetic resonance imaging. *J Am Coll Cardiol*. 2005;45:98–103.

17. Santangeli P, Pieroni M, Dello Russo A, Casella M, Pelargonio G, Macchione A, Camporeale A, Smaldone C, Bartoletti S, Di Biase L, Bellocci F, Natale A. Noninvasive diagnosis of electroanatomic abnormalities in arrhythmogenic right ventricular cardiomyopathy. *Circ Arrhythm Electrophysiol*. 2010;3:632–638.

18. Mühlenbruch G, Das M, Hohl C, Wildberger JE, Rinck D, Flohr TG, Koos R, Knackstedt C, Günther RW, Mahnken AH. Global left ventricular function in cardiac CT: Evaluation of an automated 3D region-growing segmentation algorithm. *Eur Radiol*. 2006;16:1117–1123.

19. Prakash R. Determination of right ventricular wall thickness in systole and diastole: Echocardiographic and necropsy correlation in 32 patients. *Br Heart J*. 1978;40:1257–1261.

20. Basso C, Thiene G, Corrado D, Angelini A, Nava A, Valente M. Arrhythmogenic right ventricular cardiomyopathy: dysplasia, dystrophy, or myocarditis? *Circulation*. 1996;94:983–991.

21. Garcia FC, Bazan V, Zado ES, Ren JF, Marchlinski FE. Epicardial substrate and outcome with epicardial ablation of ventricular tachycardia in arrhythmogenic right ventricular cardiomyopathy/dysplasia. *Circulation*. 2009;120:366–375.

22. Bogun F, Good E, Reich S, Elmouchi D, Igic P, Lemola K, Tschopp D, Jongnarangsin K, Oral H, Chugh A, Pelosi F, Morady F. Isolated potentials during sinus rhythm and pace-mapping within scars as guides for ablation of post-infarction ventricular tachycardia. *J Am Coll Cardiol*. 2006;47:2013–2019.

23. Santangeli P, Dello Russo A, Pieroni M, Casella M, Di Biase L, Burkhardt JD, Sanchez J, Lakkireddy D, Carbucicchio C, Zucchetti M, Pelargonio G, Themistoclakis S, Camporeale A, Rossillo A, Beheiry S, Hongo R, Bellocci F, Tondo C, Natale A. Fragmented and delayed electrograms within fibrofatty scar predict arrhythmic events in arrhythmogenic right ventricular cardiomyopathy: results from a prospective risk stratification study. *Heart Rhythm*. 2012;9:1200–1206.

24. Zeppenfeld K, Tops LF, Bax JJ, Schalij MJ. Images in cardiovascular medicine: Epicardial radiofrequency catheter ablation of ventricular tachycardia in the vicinity of coronary arteries is facilitated by fusion of 3-dimensional electroanatomical mapping with multislice computed tomography. *Circulation*. 2006;114:e51–e52.

25. Komatsu Y, Sacher F, Cochet H, Jaïs P. Multimodality imaging to improve the safety and efficacy of epicardial ablation of scar-related ventricular tachycardia. *J Cardiovasc Electrophysiol*. 2013;24:1426–1427.

26. Della Bella P, Bisceglia C, Tung R. Multielectrode contact mapping to assess scar modification in post-myocardial infarction ventricular tachycardia patients. *Europace*. 2012;14:ii7–ii12.